DIAGNOSIS OF CITRUS GREENING USING RAMAN SPECTROSCOPY-BASED PATTERN RECOGNITION**

Y. Liu*, H. Xiao, Y. Hao, L. Ye, X. Jiang, H. Wang, X. Sun

College of Mechanical and Vehicle Engineering, East China Jiaotong University, Jiangxi Province, China; e-mail: jxliuyd@163.com

This study verified the applicability of Raman spectroscopy for the detection and classification of disease in citrus leaves. The Raman spectra of citrus leaves were collected using a SENTERRA confocal microprobe Raman spectrometer and divided into five types, Huanglongbing (HLB), moderate HLB, serious HLB, nutrient deficiency, and normal. The backgrounds of the spectra were deducted by different methods, and partial least squares discrimination analysis (PLS-DA) and extreme learning machine (ELM) were used to build the mathematical model. At the same time, the data dimension was reduced using principal component analysis (PCA) and successive projection algorithm (SPA) in order to optimize and improve the classification accuracy of the model. The experiments showed that the predictive ability of the PLS-DA model with 1850 input variables by 2 times polynomial fitting deducted backgrounds was better, the recognition correct rate being 100%. The results show that Raman spectroscopy has potential for rapid diagnosis of citrus HLB.

Keywords: *citrus Huanglongbing, Raman spectroscopy, partial least squares discrimination analysis, extreme learning machine, successive projection algorithm.*

ДИАГНОСТИКА ЦИТРУСОВОГО ОЗЕЛЕНЕНИЯ С ИСПОЛЬЗОВАНИЕМ СПЕКТРОСКОПИИ КОМБИНАЦИОННОГО РАССЕЯНИЯ

Y. Liu*, H. Xiao, Y. Hao, L. Ye, X. Jiang, H. Wang, X. Sun

УДК 535.375.5:634.31/.34

Колледж машиностроения, Восточно-Китайский университет Цзяотун, Цзянси, Китай; e-mail: jxliuyd@163.com

(Поступила 26 ноября 2018)

Спектроскопия комбинационного рассеяния света использована для обнаружения бактерии Huanglongbing и классификации заболеваний листьев цитрусовых. С помощью конфокального микрозондового КР-спектрометра SENTERRA получены спектры КР листьев цитрусовых, которые разделены на пять типов: слабое, умеренное, серьезное поражение бактерией Huanglongbing, дефицит питательных веществ и нормальный уровень. Фоновые изображения спектров определены различными методами. Для построения математической модели использованы метод регрессии частных наименьших квадратов (PLS-DA) и глубокое машинное обучение (ELM). Размерность данных уменьшена использованием анализа главных компонент (PCA) и алгоритма последовательного проецирования (SPA) с целью оптимизации и повышения точности классификации модели. Лучшей прогностической способностью обладает модель PLS-DA с числом входных переменных 1850 при двукратной полиномиальной подгонке вычтенных фонов лучше, точность распознавания 100%.

Ключевые слова: *бактерия Huanglongbing у цитрусовых, спектроскопия комбинационного рассеяния света, метод регрессии частных наименьших квадратов, глубокое машинное обучение, алгоритм последовательного проецирования.*

** Full text is published in JAS V. 87, No. 1 (http://springer.com/journal/10812) and in electronic version of ZhPS V. 87, No. 1 (http://www.elibrary.ru/title_about.asp?id=7318; sales@elibrary.ru).

Introduction. Citrus greening, or Huanglongbing (HLB), is the most serious citrus disease caused by phloem-limiting bacteria. Typical symptoms in the affected leaves are described as chlorosis, blotchy mottle, and yellow veins, while the other parts of the plant show no symptoms [1–4]. It is a widespread and devastating citrus disease in the world, which seriously reduces citrus production worldwide [5]. HLB detection is a core step in disease management. The tree infected with HLB should be immediately sent back to prevent further proliferation of the disease. Thus, it is imperative that reliable techniques be developed for early and presymptomatic prompt detection [6, 7].

Currently, the two common methods are polymerase chain reaction (PCR) analysis and artificial field diagnosis. The former is very accurate and capable of identifying the disease before it becomes symptomatic. Unfortunately, this method is time-consuming and relatively expensive [8]. The latter is easy, short-cycle, but its accuracy is low. Some studies have reported that spectral techniques can be used to quickly detect HLB [9]. Sinatra et al. dried and crushed citrus leaves; then the diagnosis of leaf HLB was carried out by Fourier near-infrared spectroscopy, and the discrimination rate reached 95% [5]. Windham et al. combined it with near-infrared (NIR) spectroscopy techniques to obtain HLB positive and negative leaf spectra. The partial least squares regression model was established successfully, the classification accuracy being from 92 to 99% for HLB positive, HLB negative, and other disease and nutritional deficiency samples [10]. Deng Xiaoling et al. used hyperspectral imaging techniques to classify citrus leaves with five symptoms using principal component analysis (PCA) and back propagation neural network (BPNN), with an accuracy rate of over 90% [11]. Ma Hao et al. collected 176 hyperspectral images of citrus samples in the range ~396–1010 nm; a model of the squares support vector machine (LS-SVM) was developed, in which input variables were selected by principal component analysis (PCA) and the successive projections algorithm (SPA). The results of the model had a better classification effect with an average accuracy of 89.7 and 87.4% for three kinds of samples (healthy, HLB-affected, and zinc deficient) [12]. However, the use of Raman spectroscopy to diagnose citrus HLB has never been reported.

Raman spectra are based on the scattering effect; their peak position, intensity, and shape can reflect the structure or content information of the analyte molecules, thus achieving qualitative identification and quantitative analysis of the substances [13]. This technology is nondestructive, fast, and easy to operate; only a small sample is required and high detection sensitivity is achieved [14]. In recent years, Raman spectroscopy has been applied in plant disease detection. Tan Feng et al. used a Raman spectrometer to collect spectra of normal rice leaves and rice leaves infected with rice blast and pointed out that the slope of the spectrum peaks of attachment between the two spectra in the ranges ~828–851 and ~984–994 cm^{-1} gradually increased with disease severity, providing an effective means for the detection of rice leaf blast in early cold areas [15]. Baranski et al. used the Fourier transform Raman spectral imaging technology to conduct *in situ* nondestructive imaging detection of carotenoids in beet and celery tissues, and the results showed that when pathogens infected leaves, the amount carotenoids would decline [16].

Therefore, the major objective of this work was to explore the applicability of Raman spectroscopy techniques in the detection of HLB and the classification of disease in citrus leaves. In this study, leaves from plants were designated as infected and uninfected with HLB. The Raman spectral background of five kinds of citrus leaves was deducted by different methods, and the mathematical model was established by partial least squares discriminant analysis and the extreme learning machine. The classification ability of the model was verified using predictive samples. The experimental results show that Raman spectroscopy techniques have a great potential in the diagnosis of citrus HLB and provide a new method for the rapid detection of HLB [17–19].

Materials and methods. *Spectrometers and sample preparation.* The sample spectra were collected by a confocal microprobe Raman spectrometer (Brook Co. Ltd, Germany) with the range ~90–3500 cm^{-1}; the resolution was 9–15 cm^{-1}; the laser wavelength was 785 nm; the power was 50 nW; the integration time was 10 s; the scanning was performed 3 times, and the average was taken for further analysis.

Citrus leaves were picked in a citrus planting base in Jiangxi province. The base was divided into 5 regions, 2 trees were randomly selected with the same interval in each region, picking up 12 pieces per tree bottom-up from 4 different directions, with a total of 130 pieces; then the leaves were packed in a marked plastic bag and treated before the experiment (washed, dried, etc.). According to primers A_2/J_5 reported by Jagoueix et al. and OI_1/OI_2c reported by Hocquellet et al., the experimental samples were screened by routine PCR primers and synthesized by the Genscript Company in Nanjing [20, 21]. The sequences of A_2/J_5 and OI_1/OI_2c were 5′-GCGCGTATCCAATACGAGCGGCA-3′, 5′-GCCTCGCGACTTCGCAACCCAT-3′,

and 5′-TATAAAGGTTGACCTTTCGAGTTT-3′, 5′-ACAAAAGCAGAAATAGCACGAACAA-3′. The results were negative for diseased leaves and positive for healthy leaves (Fig. 1).

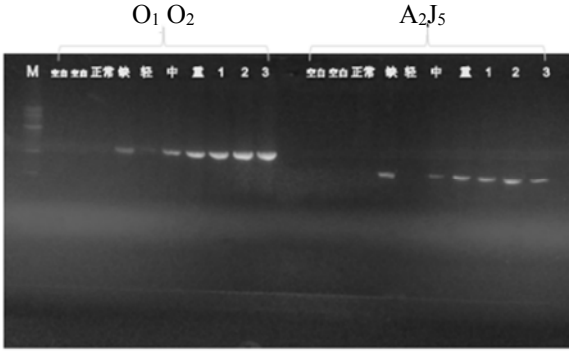

Fig. 1. The results of the polymerase chain reaction test for citrus leaves.

It can be seen that the PCR test results are better when we use OI_1/OI_2c as primers [22, 23]. Normal leaves did not show bright bands, but nutrient-deficient leaves showed bright bands due to lack of nutrients, different from HLB leaves. Samples with nutrient deficiency were selected for comparison with samples with symptoms similar to HLB, as shown in Table 1.

TABLE 1. The Category of the 26 Samples by the Polymerase Chain Reaction

Rank	Leaf infection
Normal	No symptoms of HLB, PCR test negative
Slight HLB	Slight symptoms, PCR test positive
Moderate HLB	Moderate symptoms, PCR test positive
Serious HLB	Serious symptoms, PCR test positive
Nutrient deficiency	No symptoms of HLB, PCR test negative

All the samples were divided into 5 levels, 1 was slight HLB, 2 was moderate HLB, 3 was serious HLB, 4 was nutrient deficiency, and 5 was normal [24]. Finally, the samples were numbered and await spectral analysis.

Spectra record. At normal temperature, the spectrum of the middle left area of the citrus leaf was obtained by a Raman spectrometer in a room with a humidity of ~40–50%. Throughout the process, as far as possible to keep the leaves flat and avoid veins, three spectra of each leaf were taken and averaged for subsequent data analysis.

Pattern recognition. Partial least squares discriminant analysis (PLS-DA) is widely applied in qualitative analysis to correlate the spectra matrix (X) with the related truth value (Y). PLS-DA is a linear modeling mean in which the raw independent communication (X) comes forward with a small part of the elements (also known as latent factors) to reduce the relationship between X and Y for forecasting. The forecasting Y is calculated as

$$Y = \beta X + b, \tag{1}$$

where β is a $n\times1$ matrix of regression coefficients, and b is the model bias. The extreme learning machine (ELM) is a new algorithm for the single hidden layer feedforward neural network. It randomly generates the connection weight of the input layer, the hidden layer, and the threshold of hidden layer neurons. It does not need to be adjusted during training, and the number of hidden layer neurons was set to get the only optimal solution [25].

Results and discussion. *Raman shift analyses.* In the experiment, the Raman spectra of slight HLB, moderate HLB, serious HLB, nutrient deficiency, and normal citrus leaves were obtained in the range 90–3500 cm^{-1}, and the typical spectra are shown in Fig. 2a. It can be seen that there was an obvious characteristic peak at 1526 cm^{-1}, which may be caused by the stretching vibration of the C=C double bond of the leaves. The diseased leaves were attacked by bacteria and lack of water, resulting in the reduction of the C=C double bond stretching vibration. Thereby the characteristic peaks were lower than in the normal leaves

and decreased with severity of the disease [15]. Nutrient-deficient leaves may be deficient in some nutrient elements, leading to characteristic peaks below the customary but higher than HLB leaves not affected by pathogens.

The content of the effective information in the leaf spectra was small owing to the environment influence. Therefore, the spectrum in the ranges 90–714.5 and 1640–3500 cm^{-1} was removed. The typical spectrum in the range 715–1639.5 cm^{-1} is presented in Fig. 2b. We observed a significant characteristic maximum at 1155 cm^{-1}. Meanwhile, it was larger than the one for the leaves with HLB, which may be caused by the C-C single bond stretching vibration.

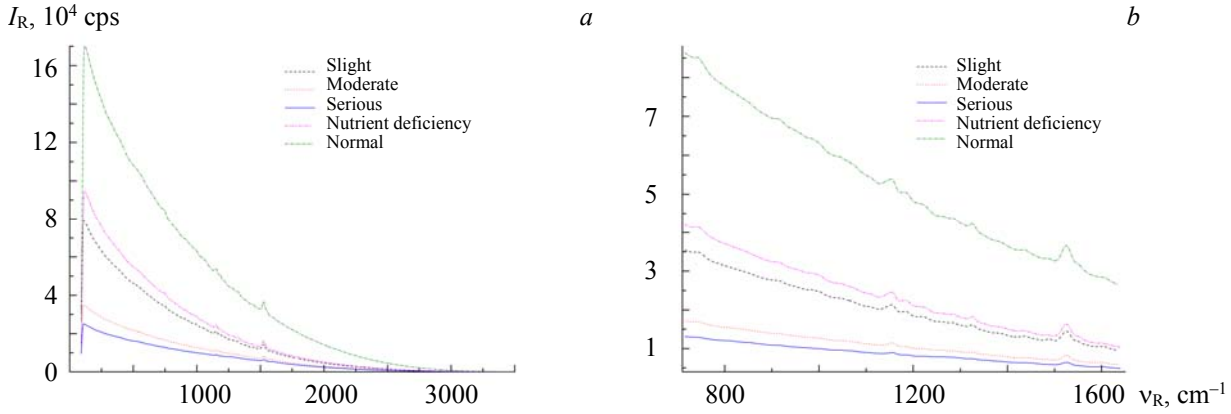

Fig. 2. Raman spectra of 5 kinds of leaves in wavelength ranges 90–3500 (a) and 715.0–1639.5 cm^{-1} (b).

Spectral baselines removal. It was necessary to deduct the background in order to make the characteristic spectral maxima more obvious and facilitate clustering analysis. The principal derivative and linear fitting methods were used to deduct the spectral background. The illustrative spectra after subtracting the background by 1 derivative with a window width of 5 points are shown in Fig. 3. There are characteristic maxima for 1155 and 1526 cm^{-1}. This indicates that the method preserves the original effective information.

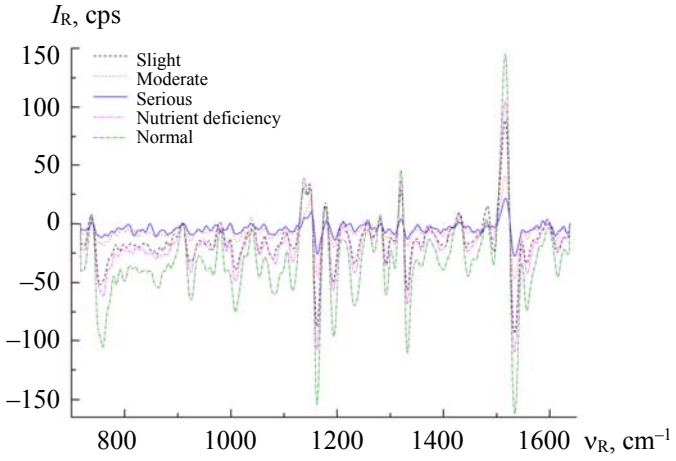

Fig. 3. Raman spectra of 5 kinds of leaves after 1 derivative with a window width of 5 points.

Linear fitting can eliminate the stray light and noise for ensuring the operational information of the sample. We applied the process of polynomial linear fitting to the spectrum before and after the background subtraction. The sample spectra obtained after polynomial fittings are shown in Fig. 4. It can be seen that in this case the spectral characteristic maxima of the samples are more obvious than for the original spectrum at 1155 and 1526 cm^{-1}, and the frequency shift position of the original Raman peak is the same. Thus, the proposed method does not delete valid information [26, 27].

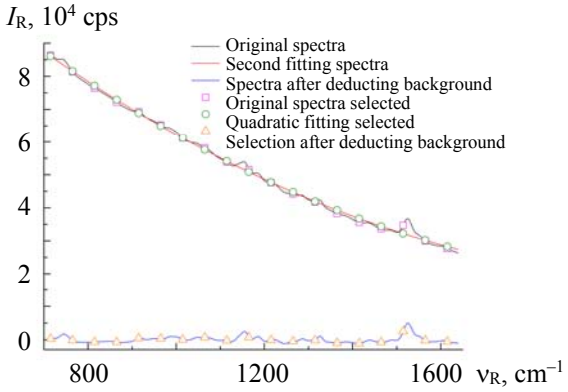

Fig. 4. The Raman spectra of the samples after 2 polynomial fittings.

Below are presented the formulas for 2, 3, 4 times polynomial fittings, and the spectral background deduction equation:

$$Y = k_{i1}x^2 + k_{i2}x + k_i\,,\ i = 1,\cdots, 104\,, \tag{2}$$

$$Y = m_{i1}x^3 + m_{i2}x^2 + m_{i3}x + m_i\,,\ i = 1,\cdots, 104\,, \tag{3}$$

$$Y = n_{i1}x^4 + n_{i2}x^3 + n_{i3}x^2 + n_{i4}x + n_i\,,\ i = 1,\cdots, 104\,, \tag{4}$$

$$Y_1 = Y_2 - Y\,, \tag{5}$$

where Y is the spectral intensity of N times polynomial fitting, x is the wave number in the range 715–1639.5 cm^{-1}, and Y_1, Y_2 are the spectral intensities before and after subtracting the background.

Spectral dimension reductions. As a rule, the object of analysis is characterized by a set of many variables. We used the PCA and SPA to simplify the investigation of Raman leaf spectra.

PCA is a typical statistical analysis method in which one uses a few comprehensive indicators without losing the original information [28]. We assumed that the maximal number of principal components is 20, so the matrix of 1850 variables before and after the spectral fittings is compressed into linear combinations of 20 principal components. Figure 5 shows the score of the first 3 principal components (PCs). It can be observed that normal samples and the sample with slight HLB can be roughly separated, but it is difficult to distinguish the cross between 3 kinds of samples including moderate HLB, serious HLB, and nutrient deficiency. Although the cumulative contribution rate of the first 3 PCs is 99%, it cannot be judged accurately on the samples and categories of HLB. Therefore, PLS-DA and ELM qualitative analysis was applied to improve the model and the accuracy of discrimination.

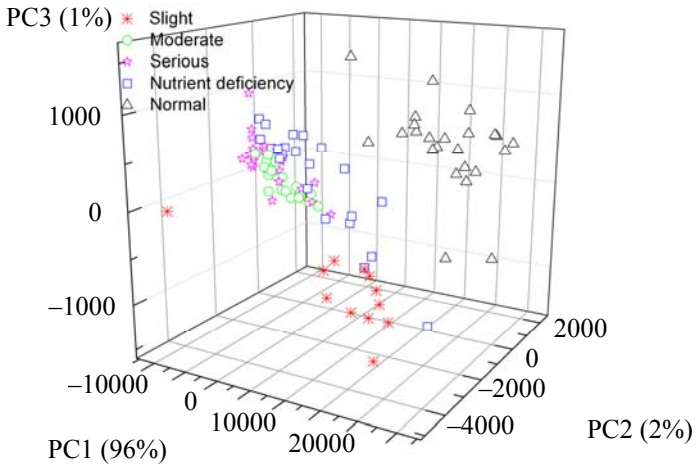

Fig. 5. The Raman spectra score projection of the first three PCs of all leaves.

The SPA is a forward wavelength selection method by which the projection of the previous wavelength in the unselected wavelength is calculated in each cycle, and the wavelength with the maximum projection is applied to the wavelength combination to reduce the linear relationship with the previous wavelength. It can effectively eliminate the influence of multivariate correction collinearity, simplify the calculation, and reduce the dimension of the spectral matrix, and it has been widely used for quantitative and qualitative analysis of spectral data [29]. In this paper, the minimum and maximum variables were placed at 1 and 30, respectively. The variables were screened by the successive projection algorithm in Matlab 2010a software for the sample spectra before and after the fittings (the results are shown in Figs. 6a,b); 25 and 15 cm^{-1} wavenumbers were obtained, respectively. As a characteristic wavelength combination variable, the partial least squares discriminant analysis and extreme learning machine model are established, based on the true value. The results are analyzed.

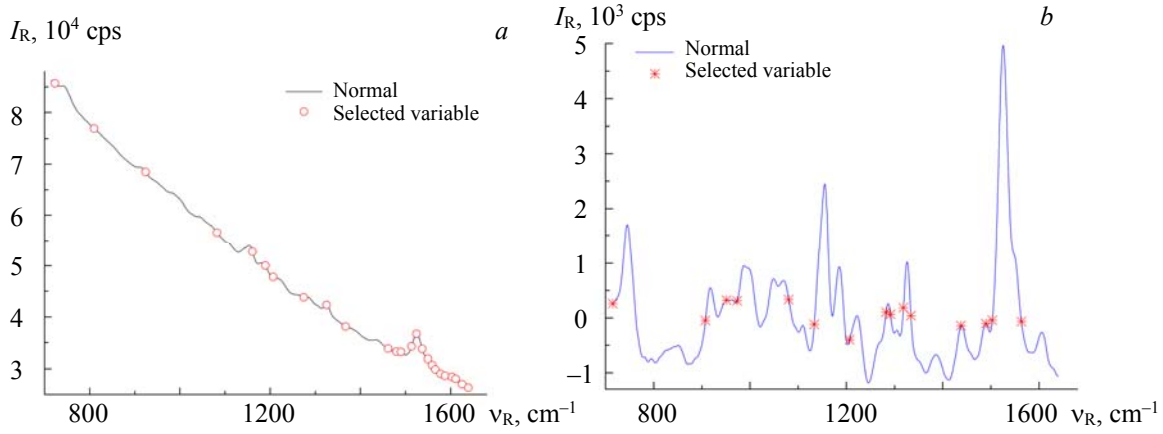

Fig. 6. The results of the SPA screening before (a) and after (b) spectral fitting.

Discrimination models. In order to make the spectra correct and not affect the results of the ensuing model, 26 samples damaged in the storage process were eliminated. There were 13 slight HLB, 7 moderate HLB, 4 nutrient deficient, and 2 normal leaves. The remaining 104 samples were divided into a calibration set and a prediction set with a ratio of 4:1. The former contains 84 samples (8 samples are slight HLB, 15 samples are moderate HLB, 23 samples are serious HLB, 18 samples are nutrient deficient, and 20 samples are normal). The latter 20 samples are used for evaluation of the effect of the model. Slight HLB, moderate HLB, serious HLB, nutrient deficient, and normal samples were assumed to be 2, 4, 6, 8, and 10, respectively; the median values were taken as the classification thresholds.

A PLS-DA model was developed with 1850 input variables in the range 715–1639.5 cm^{-1} by the two methods above to deduct the spectral background. The predictive effect of the PLS-DA model was studied with the help of the prediction set samples to choose the best method of deducting the background. Table 2 shows that the model of twice fitting was the best. The correct recognition rate was 100%, the maximum correlation coefficient of prediction was 0.98, and the minimum root mean square error of prediction was 0.67; therefore, the spectral background was deducted by this method.

TABLE 2. The Statistical Results of the Partial Least Squares Discriminant Analysis Model

Background deduction methods	The best PCs	RMSEP	R_P	Correct recognition rate,%
None	12	0.69	0.98	95
1 derivative with a window width of 5 points	5	0.93	0.95	70
2 times fitting	10	0.67	0.98	100
3 times fitting	9	0.77	097	95
4 times fitting	8	0.82	0.97	95

The best principal component factor was used as one of the highest performance indexes of the model, and the leave-one-out method was used to determine the optimum number. The number of the principal component factor of the best model decision diagram is shown in Fig. 7a. It can be seen that the root means square error decreases with increasing number of factors. But the root mean square error of the prediction set reaches the minimum for 10, and then increases, so the optimal number of the principal components factor of the PLS-DA model is determined as 10.

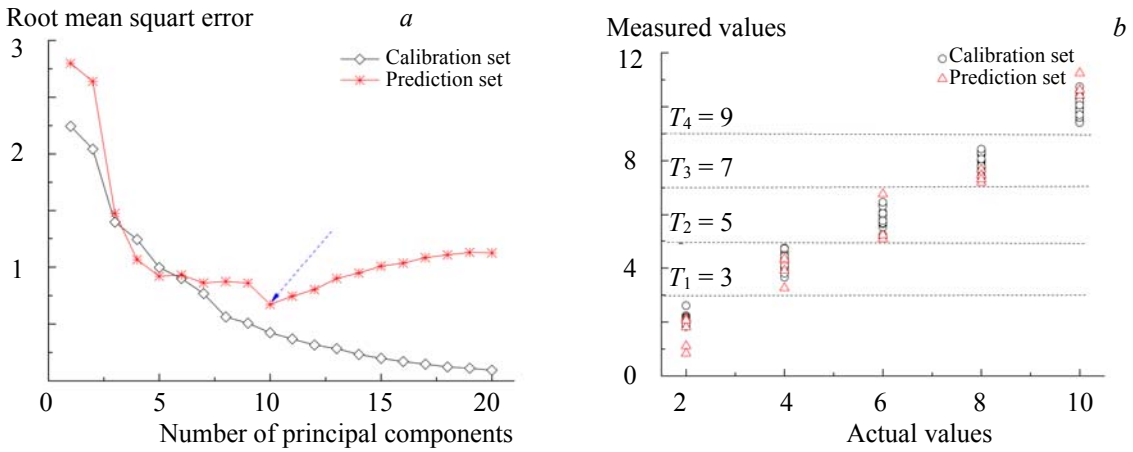

Fig. 7. The results of the best PLS-DA model: (a) the optimal PCs number decision map, (b) the scatter diagram of the model.

The scatter diagram of the best PLS-DA model for the mid-value of two levels of classification is presented in Fig. 7b. For further optimization of the model, we developed two variable selective methods of PCA and SPA before and after twice fitting the spectra. The results are shown in Table 3. It can be seen that the effect of the model was better when the PCA compression variables were input before twice fitting. Meanwhile, the correct recognition rate was 95%, the root mean square error of prediction was 0.73, and the prediction correlation coefficient was 0.98. Compared to the PLS-DA model for the full spectrum after the fitting, although the number of input variables and principal components was small, the correct recognition rate was lower than for the latter, so the effect of the PLS-DA model for the full spectrum was the best after twice fitting.

During the training period, the ELM network tends to produce a cover fitting phenomenon. To avoid this situation, the number of hidden layer neurons in the ELM network should be determined before training, and the weight variable and node offset should be assigned randomly. In this experiment, the number of hidden layer neurons was initialized to 10, and the step size was 10, gradually raised to 80. The number of hidden layer neurons was the best at the highest correct recognition rate. There are functions, including sine, sigmoidal, and Hardlim training, with the number of hidden layer neurons being determined for the optimal excitation function, respectively [30–32]. The influence of different numbers of hidden layer neurons on the ELM performance is shown in Fig. 8. It can be seen that the correct recognition rate increases with increase in the number of neurons. For example, when the number of neurons was 50, the correct recognition rate reached its maximum. Meanwhile, the correct recognition rate of sigmoidal as the excitation function was the highest (90%). Therefore, the follow-up ELM network model takes sigmoidal as the excitation function, and the number of hidden layer neurons is 50.

TABLE 3. The Results of the PLS-DA Model by Different Variables before and after Twice Fittings

Spectra background	Variable selection method	The best PCs	RMSEP	R_P	Correct recognition rate,%
Before fitting	PCA	7	0.81	0.98	95
	SPA	13	0.8	0.97	85
After fitting	PCA	5	0.73	0.98	95
	SPA	11	1.14	0.96	80

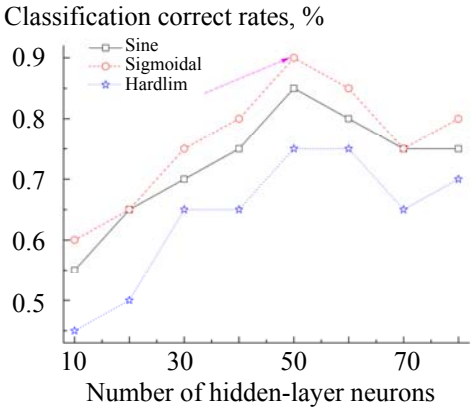

Fig. 8. Relation between the correct recognition rate and the number of hidden-layer neurons on 3 functions.

The ELM recognition model was established with input variables before and after spectral fittings in the full band range. The variables selected by PCA and SPA were used as input to optimize the model. The results were evaluated without modeling samples. The specific results are shown in Table 4.

Three ELM models can better determine HLB before and after the spectral fittings according to the results from Table 4. However, the correct recognition rate of the model was 95% with the full spectrum as the input after the spectral fitting. The root mean square error of prediction was 0.73, and the correlation coefficient was 0.9736. The model of the SPA filter variable was the worst, probably due to the loss of some information during the screening of variables. Although the number of variables of the full spectrum for the model input was large, the effect was better than for the rest of the models. So, the ELM model was better after twice spectral fittings.

TABLE 4. Prediction Results of the ELM Model in Different input Variables before and after Twice Fittings

Spectra background	Number of input variables	Selecting method	RMSEP	R_P	Classification correct rate,%
Before fitting	1850	None	0.86	0.9483	90
	20	PCA	0.92	0.9109	90
	25	SPA	1.04	0.8811	85
After fitting	1850	no	0.73	0.9736	95
	20	PCA	0.85	0.9519	90
	15	SPA	0.94	0.9430	85

The results of the investigation are the following. The prediction accuracy of the PLS-DA model of 1850 variables was the most accurate. At this time, the number of PC was 10, the prediction correlation coefficients and errors were 0.98 and 0.67, respectively, and the correct recognition rate was 100%. The effect of the ELM model full spectrum after twice fittings as the input was better with sigmoidal as the excitation function, the correlation coefficient of the prediction set was 0.9736, the error was 0.73, and the correct recognition rate was 95%. The model after twice fitting was better than before fitting.

Conclusion. The Raman spectra background of citrus leaves were deducted by the first derivative and linear fitting, and the spectral peaks were highlighted. The spectra variable was screened using the PCA and SPA methods in the range 715.0–1639.5 cm^{-1}. The partial least squares discriminant analysis and extreme learning machine models were successfully applied for speedy diagnosis of citrus HLB. We found that the classification effect of the partial least square discriminant analysis model with 1850 input variables after twice fittings was the best for 5 kinds of samples. The best principal component factor was 10, and the correct recognition rate was 100%. The study shows that the combination of Raman spectra and PLS-DA can be used to explore the feasibility of prompt diagnosis of HLB and provide another way for the study of nondestructive detection of citrus HLB.

Acknowledgment. The research was funded by the National Natural Science Foundation of China (No. 31760344), the Center of the Technology and Equipment of the Intelligent Management for the South-

ern Mountain Orchard Collaborative Innovation (No. 2014-60), the Jiangxi Advantage Science and Technology Innovation Team Construction Project (No. 20153BCB24002), the Special../anzhuang/youdao/Dict/7.5.2.0/resultui/dict/?keyword= Project of Innovation Ability for Jiangxi Province (No. [2016]1074), the Photoelectric Inspection Engineering Technology Research Center of Jiangxi Province (No. 20161BCD40021), and the Youth Project of Jiangxi Province Education Department (No. GJJ160517).

REFERENCES

1. S. Saharan, J. M. Maja, S. Buchanon, R. Ehsani, *Sensors*, **13**, No. 2, 2117–2130 (2013).
2. X. L. Deng, Y. D. Gao, J. C. Chen, X. L. Pu, W. W. Kong, H. P. Li, *J. Integr. Agric.*, **11**, No. 3, 424–429 (2012).
3. J. M. Bové, *Phytoparasitica*, **42**, No. 5, 579–583 (2014).
4. A. Mitra, D. Karimi, R. Ehsani, L. G. Albrigo, *Biosystem. Eng.*, **110**, No. 3, 302–309 (2011).
5. S. Saharan, R. Ehsani, *Crop Protect.*, **30**, No. 11, 1508–1513 (2011).
6. S. A. Hawkins, B. Park, G. H. Poole, T. Gottwald, W. R. Windham, K. C. Lawrence, *Appl. Spectrosc.*, **64**, No. 1, 100–103 (2010).
7. S. Saharan, R. Ehsani, E. D. Etxeberria, *Talanta,* **83**, No. 2, 574–581 (2010).
8. X. H. Li, W. S. Lee, M. Z. Li, R. Ehsani, A. R. Mishra, C. H. Yang, R. L. Mangan, *Comput. Electron. Agric.*, **83**, 32–46 (2012).
9. S. Saharan, R. Ehsani, *Agric. Eng. Int.: CIGR J.*, **15**, No. 3, 75–79 (2013).
10. W. R. Windham, G. H. Poole, B. Park, G. Heitschmidt, S. A. Hawkins, J. P. Albano, T. R. Gottwald, K. C. Lawrence, *Trans. ASABE*, **54**, 2253–2258 (2011).
11. X. L. Deng, C. Kong, W. B. Wu, H. L. Mei, Z. Li, T. S. Hong, *Acta Photon. Silica*, **43**, No. 4, 16–22 (2014).
12. H. Ma, H. Y. Ji, W. S. Lee, *Spectrosc. Spectr. Anal.*, **36**, No. 7, 2344–2350 (2016).
13. Y. J. Xu, R. H. Luo, M. T. Guo, J. F. Wu, M. Y. Li, *Laser J.*, **28**, No. 2, 13–14 (2007).
14. N. Wei, X. Q. Feng, X. F. Zhang, X. H. Qi, M. Q. Zou, M. T. Wang, *Spectrosc. Spectr. Anal.*, **33**, No. 3, 694–698 (2013).
15. F. Tan, Q. L. Cai, X. C. Sun, Z. X. Ma, Z. L. Hou, *Transact. Chin. Soc. Agric. Eng.*, **31**, No. 4, 191–196 (2015).
16. R. Baranski, M. Baranska, H. Schulz, *Planta*, **222**, No. 3, 448–457 (2005).
17. A. Parrish, W. S. Lee, E. D. Etxeberria, A. Banerjee, *Biosystem. Eng.*, **130**, 13–22 (2015).
18. F. G. Ruiz, S. Sankaran, J. M. Maja, W. S. Lee, J. Rasmussen, R. Ehsani, *Comput. Electron. Agric.*, **91**, 106–115 (2013).
19. J. Gonzalezmora, G. Vallespi, C. S. Dima, *10th ICPA Proc. Mora* (2010).
20. X. Deng, G. Zhou, H. Li, J. Chen, E. L. Civerolo, *Plant Dis.*, **91**, No. 8, 1051–1054 (2007).
21. A. Hocquellet, P. Toorawa, J. M. Bove´, M. Garnier, *Mol. Cell. Probes*, **13**, No. 5, 373–379 (1999).
22. T. Li, C. Ke, *Acta Phytophylac. Silica*, **1**, 31–35 (2002).
23. X. H. Li, M. Z. Li, W. S. Lee, R. Ehsani, A. R. Mishra, *Spectrosc. Spectr. Anal.*, **34**, No. 6, 1553–1559 (2014).
24. Y. W. Yuan, Z. Z. Jiang, D. S. Wang, *Zhejiang Agric. Sci.*, **1**, 121–123 (2010).
25. W. B. Zheng, X. P. Fu, Y. B. Ying, *Chemom. Intell. Lab. Syst.*, **139**, 42–47 (2014).
26. Z. J. Qin, Z. H. Tao, J. X. Liu, G. W. Wang, *Spectrosc. Spectr. Anal.*, **33**, No. 2, 383–386 (2013).
27. X. Su, S.Y. Fang, D. S. Zhang, Y. He, *J. Biomed. Opt.*, **20**, No. 12, 1117–1124 (2015).
28. L. Y. Gong, X. J. Meng, N. Q. Liu, J. F. Bi, *Trans. Chin. Soc. Agric. Eng.*, **30**, No. 13, 276–285 (2014).
29. Y. Yuan, W. Wang, X. Chu, M. J. Xi, *Spectrosc. Spectr. Anal.*, **36**, No. 1, 226–230 (2016).
30. H. D. Zhang, G. R. Li, R. C. Li, W. F. Xu, Y. J. Hua, *Laser Optoelectron. Progr.*, **4**, 183–189 (2013).
31. W. C. Guo, M. H. Wang, J. S. Gu, X. H. Zhu, *Opt. Precis. Eng.*, **10**, 2720–2727 (2013).
32. J. Sun, A. G. Wei, H. P. Mao, X. H. Wu, X. D. Zhang, *Trans. Chin. Soc. Agric. Mach.*, **7**, 272–277 (2014).